Volume 17
Number 19
20 May 2026
Pages 9313–9798

Chemical Science

rsc.li/chemical-science

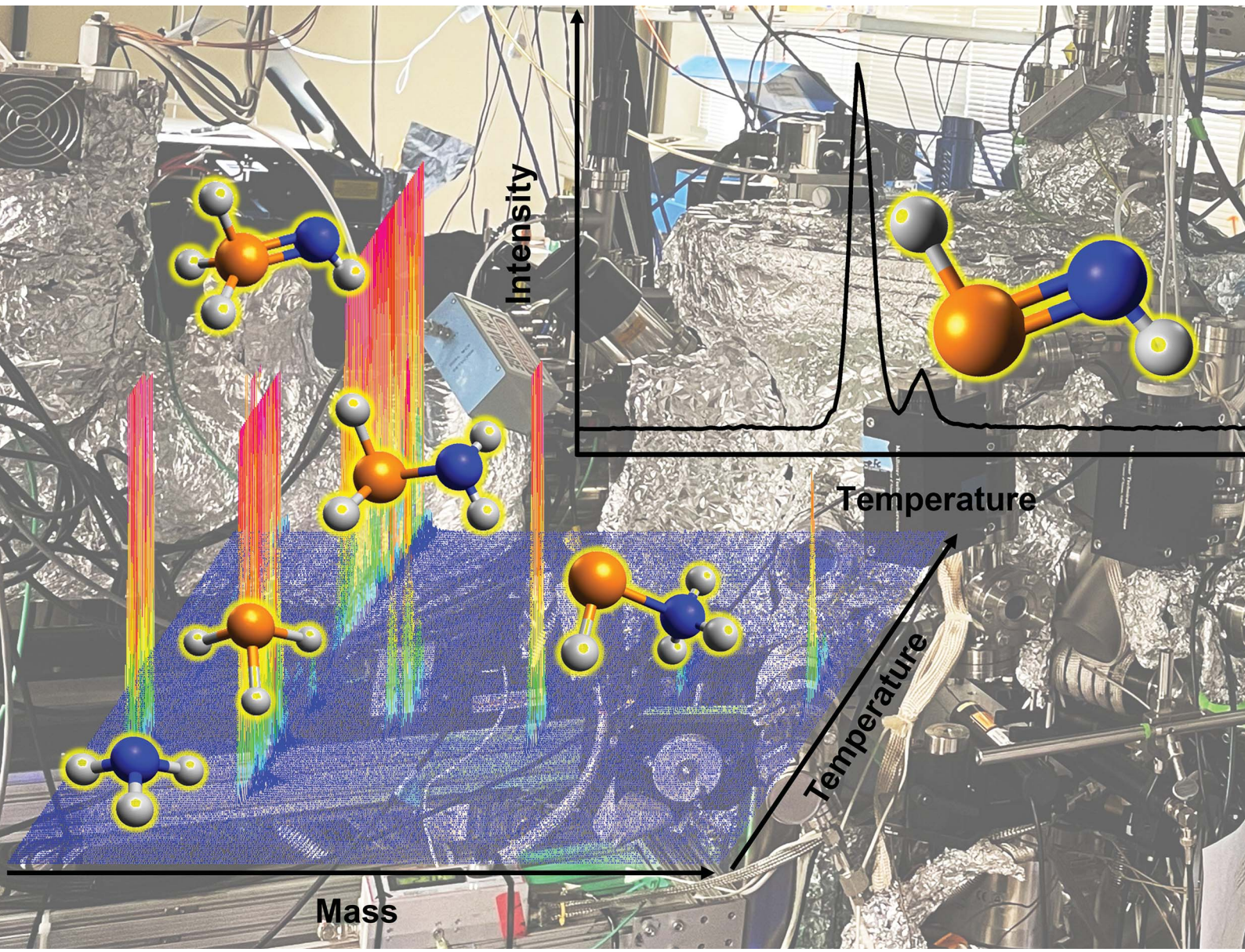

ISSN 2041-6539

ROYAL SOCIETY OF CHEMISTRY

EDGE ARTICLE

Agnes H. H. Chang, André K. Eckhardt, Ralf I. Kaiser *et al.*
Non-equilibrium preparation of (*E*)-phosphinimine (HPNH, X^{1}A′) – a precursor to prebiotic phosphorylating agents

Chemical Science

ROYAL SOCIETY OF CHEMISTRY

EDGE ARTICLE

View Article Online
View Journal | View Issue

Cite this: *Chem. Sci.*, 2026, **17**, 9446

All publication charges for this article have been paid for by the Royal Society of Chemistry

Non-equilibrium preparation of (*E*)-phosphinimine (HPNH, X^1A') – a precursor to prebiotic phosphorylating agents

Jia Wang, [ab] Bing-Jian Sun,[c] Alexandre Bergantini, [ab]† Zesen Wang,[ab] Mason McAnally, [ab] Joshua H. Marks,[ab] Agnes H. H. Chang,*[c] André K. Eckhardt *[d] and Ralf I. Kaiser *[ab]

Received 4th March 2026
Accepted 28th April 2026

DOI: 10.1039/d6sc01818a

rsc.li/chemical-science

Phosphorus–nitrogen compounds play crucial roles as intermediates in aza-Wittig reactions and serve as key precursors to prebiotic phosphorylating agents such as amidophosphonates linked to the Origins of Life. However, their formation mechanisms under astrophysical conditions remain largely unexplored. Here, we report the first formation of (*E*)-phosphinimine (HPNH, X^1A') – the simplest iminophosphane – in low-temperature interstellar model ices composed of phosphine (PH_3) and ammonia (NH_3) exposed to galactic cosmic ray proxies in the form of high-energy electrons. Utilizing vacuum ultraviolet photoionization reflectron time-of-flight mass spectrometry in tandem with computed adiabatic ionization energies permits the very first identification of (*E*)-phosphinimine in the gas phase during the temperature-programmed desorption of irradiated ices. Our study reveals a critical formation pathway for iminophosphanes *via* non-equilibrium chemistry through nitrogen- and phosphorus-centered radicals in interstellar environments preceding the formation of stars and planets thus affording useful insights into the interstellar phosphorus–nitrogen chemistry essential for the origin of prebiotic molecules.

Introduction

Ever since the detection of the first interstellar phosphorus-containing molecule—phosphorus mononitride (PN)—nearly four decades ago,[1,2] phosphorus-bearing molecules have attracted significant attention from the astrochemistry,[3] astrobiology,[4] theoretical chemistry,[5–8] and physical organic chemistry communities[9–11] due to their essential role in the synthesis of prebiotic biomolecules such as phospholipids, adenosine triphosphate (ATP), and ribonucleic acid (RNA).[12] Among the eight phosphorus-bearing molecules identified in the interstellar medium (ISM)—PN, phosphinidynemethyl (CP), phosphaethyne (HCP), phosphorus monoxide (PO) plus its cation (PO^+), phosphinidyneethylidyne (CCP), phosphine (PH_3), silicon phosphide (SiP)[13,14]—PN and PO are contemplated to play a key role in the evolution of the phosphorus chemistry in molecular clouds and star-forming regions.[5,15,16] Additionally, phosphorus-bearing molecules have been delivered to early Earth as evidenced by the detections of PO in comet 67P/Churyumov–Gerasimenko[17] and organic alkylphosphonic acids (RPO_3H_2, $R = C_nH_{2n+1}$) and inorganic phosphates (PO_4^{3-}) in the Murchison meteorite,[18] which was formed approximately 7 billion years ago.[19] Thus, elucidating the formation pathways of phosphorus-containing molecules is essential for understanding how phosphorus-based biochemistry, and potentially the molecular Origins of Life, might have emerged on early Earth.[20] However, the interstellar chemistry of phosphorus has remained poorly understood,[8,13] particularly from the viewpoint of the synthesis of phosphorus–nitrogen-containing (P–N) molecules under extreme circumstellar and interstellar conditions.

Phosphorus–nitrogen moieties serve not only as potential precursors to prebiotic phosphorylating agents such as amidophosphonate ($HOP(O)HNH_2$) and diamidophosphate ($HOP(O)(NH_2)_2$) linked to Origins of Life,[21] but also as key intermediates in aza-Wittig reactions,[22] contributing to the synthesis of biorelevant heterocyclic compounds.[23] Additionally, they also provide fundamental insights into electronic structure and chemical bonding.[24,25] Under astrophysical conditions, these species may form *via* non-equilibrium chemistry driven by galactic cosmic rays (GCRs) and vacuum ultraviolet (VUV) radiation in exposed phosphine (PH_3) and ammonia (NH_3)-containing interstellar ices. Laboratory experiments have demonstrated the abiotic formation of

[a]*W. M. Keck Research Laboratory in Astrochemistry, University of Hawaii at Manoa, Honolulu, Hawaii 96822, USA. E-mail: ralfk@hawaii.edu*

[b]*Department of Chemistry, University of Hawaii at Manoa, Honolulu, Hawaii 96822, USA*

[c]*Department of Chemistry, National Dong Hwa University, Shoufeng, Hualien 974, Taiwan. E-mail: hhchang@gms.ndhu.edu.tw*

[d]*Lehrstuhl für Organische Chemie II, Ruhr-Universität Bochum, Bochum 44801, Germany. E-mail: Andre.Eckhardt@rub.de*

† Present address: Centro Federal de Educacao Tecnologica Celso Suckow da Fonseca-CEFET-RJ, Av. Maracana 229, 20271-110, Rio de Janeiro, Brazil.

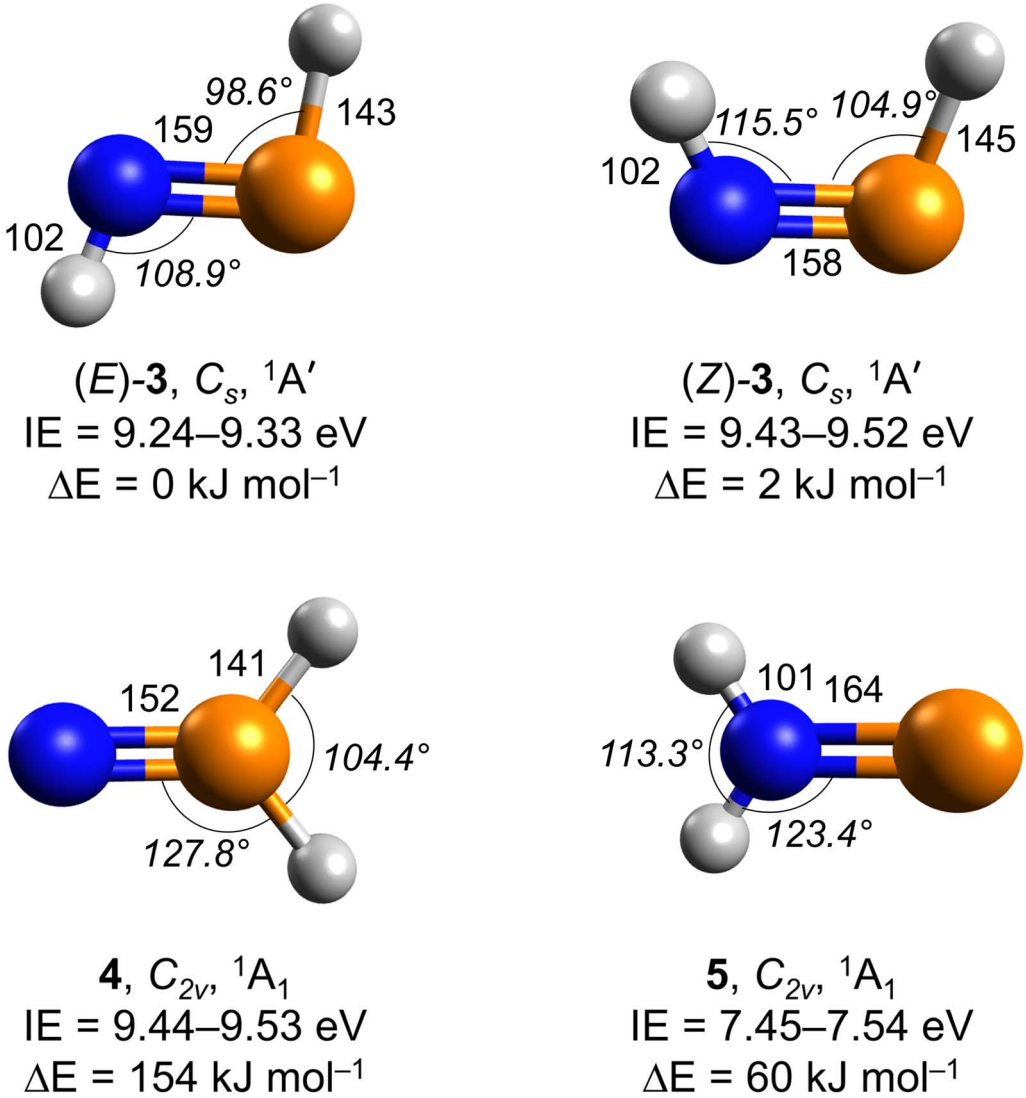

Fig. 1 Optimized molecular structures of H_2NP isomers: phosphinimine ((*E*)-**3** and (*Z*)-**3**), phosphinonitrene (**4**), and iminophosphinidene (**5**). Bond length (in pm), bond angles (in italic), point group symmetries, electronic ground states, adiabatic ionization energies (IEs), and relative energies (Δ*E*) are shown (Table S2). Atomic color coding: hydrogen (white), nitrogen (blue), and phosphorus (orange).

phosphinous amide (H_2PNH_2, X^1A, **1**) and phosphine imide (H_3PNH, X^1A_1', **2**) from low-temperature phosphine–ammonia ice mixtures.[3] Prismatic P_3N_3 and cyclotriphosphazene (*c*-P_3N_3) were synthesized by exposing phosphine–nitrogen (PH_3–N_2) ices with GCR proxies in the form of energetic electrons,[24,25] indicating plausible routes leading to strained cage molecules.[24] However, the formation pathways of P–N moieties linked to the Origins of Life have just scratched the surface, and even the interstellar formation of the simplest iminophosphane – phosphinimine (HPNH, X^1A', **3**) – has remained elusive to date. In the gas phase, **3** exists in (*E*) and (*Z*) forms with the (*E*) structure energetically favored by 2 kJ mol^{-1} (Fig. 1). Electronic structure calculations of distinct H_2PN isomers predict that (*E*)-**3** is kinetically stable considering high barriers to isomerization exceeding 250 kJ mol^{-1} *de facto* blocking hydrogen shifts to phosphinonitrene (NPH_2, X^1A_1, **4**) and iminophosphinidene (H_2NP, X^1A_1, **5**) in the gas phase.[6,26] Hence, these barriers are sufficient to allow for the existence of phosphinimine (HPNH, **3**).

Here, we report the first preparation of (*E*)-phosphinimine ((*E*)-**3**) – the phosphorus analog of diazene (HNNH) – in low-temperature (5 K) interstellar model ices composed of phosphine and ammonia. The ice mixtures were exposed to energetic electrons, simulating secondary electrons produced by GCRs when penetrating interstellar ices.[27] The applied irradiation dose is equivalent to $(2 \pm 1) \times 10^6$ years of GCRs exposure on interstellar ices, corresponding to the early stages of a molecular cloud.[28] Isomer (*E*)-**3** was identified in the gas phase during the temperature-programmed desorption (TPD) of irradiated ices utilizing vacuum ultraviolet photoionization reflectron time-of-flight mass spectrometry (PI-ReToF-MS) supported by computed adiabatic ionization energies (IEs) and isotopic labeling experiments. These findings reveal critical formation pathways leading to (*E*)-**3** *via* non-equilibrium chemistry in

extraterrestrial ices involving phosphorus–nitrogen bond coupling followed by oxidation and hence inherent hydrogen loss. Phosphine has been detected in the gas phase in the ISM at abundances up to 4×10^{-7} relative to molecular hydrogen (H_2),[29,30] and is believed to form efficiently on interstellar nanoparticles (grains) *via* successive hydrogenation of atomic phosphorus.[17,31] Ammonia is a ubiquitous constituent of interstellar ices[32] with estimated abundances up to 15% relative to water.[33] The phosphine–ammonia ices therefore represent a model system to investigate the formation mechanism of H_2PN isomers in the ISM. Our results suggest that (*E*)-**3** can form in interstellar ices containing phosphine and ammonia, making it a potential target for future astronomical observations. Once formed, it may serve as a key precursor to nitrogenous analogues of biorelevant phosphates such as amidophosphonate,[21] thereby providing new insight into the formation mechanisms of P–N moieties in extraterrestrial environments and the broader evolution of phosphorus chemistry in deep space.

Results and discussion

Fourier transform infrared (FTIR) spectra of phosphine–ammonia ices were recorded before, during, and after irradiation at 5 K with energetic electrons (Fig. S1 and Table S1). In the experiments, low-dose electron irradiation (20 nA for 15 minutes) was employed to minimize sequential reactions, thereby limiting the possible formation pathways leading to H_2NP isomers. The amino radical ($^{\bullet}NH_2$) is observable by its N–H bending mode[33,34] at 1504 cm^{-1}. Isodiazene (N=NH_2) is identified tentatively based on its N–H stretching mode (ν_5)[34] at 2768 cm^{-1}. Absorptions at 2236 and 1100 cm^{-1} are respectively assigned to the P–H and P=N stretching modes.[3,35] The latter feature may be attributed to (*E*)-**3** as well as other phosphorus–nitrogen-containing species. However, due to overlapping absorption bands from various irradiation products, FTIR spectroscopy alone cannot unambiguously identify other products,[36] highlighting the need for an alternative, isomer-specific technique to identify individual reaction products.[37]

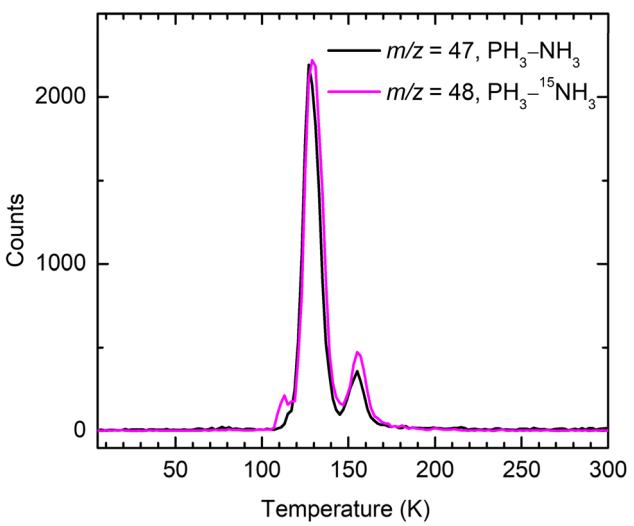

Fig. 2 Temperature-programmed desorption (TPD) profiles of irradiated phosphine–ammonia ices collected at 10.49 eV. TPD profiles of $m/z = 47$ and 48 originate from irradiated PH_3–NH_3 and PH_3–$^{15}NH_3$ ice, respectively.

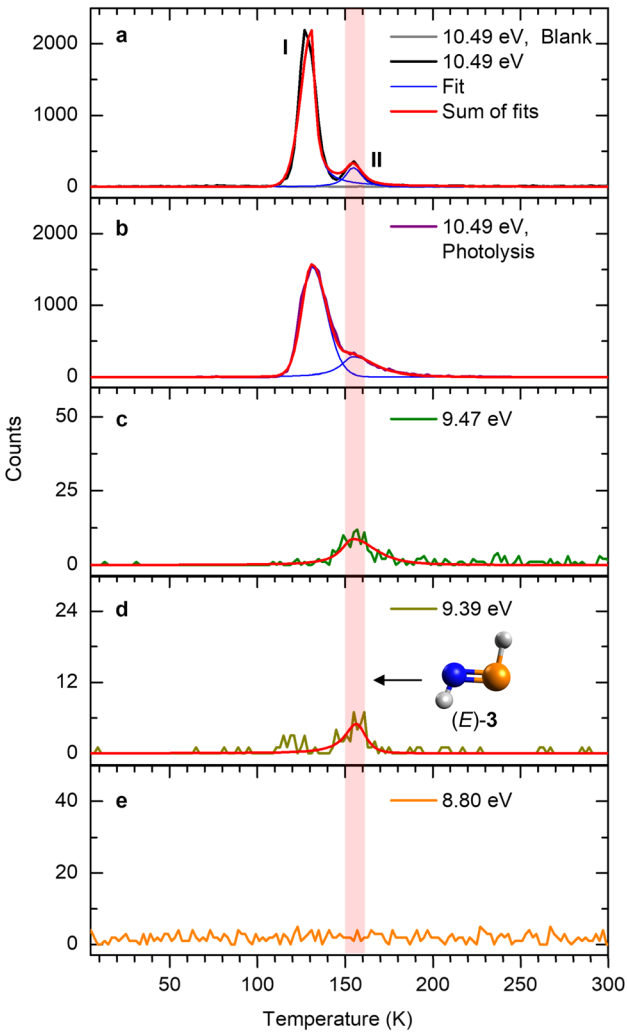

Fig. 3 TPD profiles of ion signal at $m/z = 47$ from irradiated PH_3–NH_3 ices. TPD profiles were measured at photon energies of 10.49 eV (a and b), 9.47 eV (c), 9.39 eV (d), and 8.80 eV (e). At 10.49 eV, the TPD profile of $m/z = 47$ exhibits two distinct sublimation events as fitted with peaks I and II. The red shaded region indicates the peak sublimation temperature attributed to (*E*)-**3**.

The PI-ReToF-MS technique was utilized in combination with isotopic labeling to detect H_2PN isomers based on their mass-to-charge ratios (m/z) and IEs. At a photon energy of 10.49 eV, the TPD profile of the ion signal at $m/z = 47$ from irradiated PH_3–NH_3 ice reveals two sublimation events: an early peak at 127 K (peak I) and a later, low-intensity peak at 153 K (peak II) (Fig. 2 and 3). A blank experiment was performed under identical conditions but without electron irradiation of the PH_3–NH_3 ice; no sublimation event was observed at $m/z = 47$, indicating that both sublimation events originate from electron-induced processing of the ice. Given the molecular weights of the reactants, the ion signal of $m/z = 47$ could

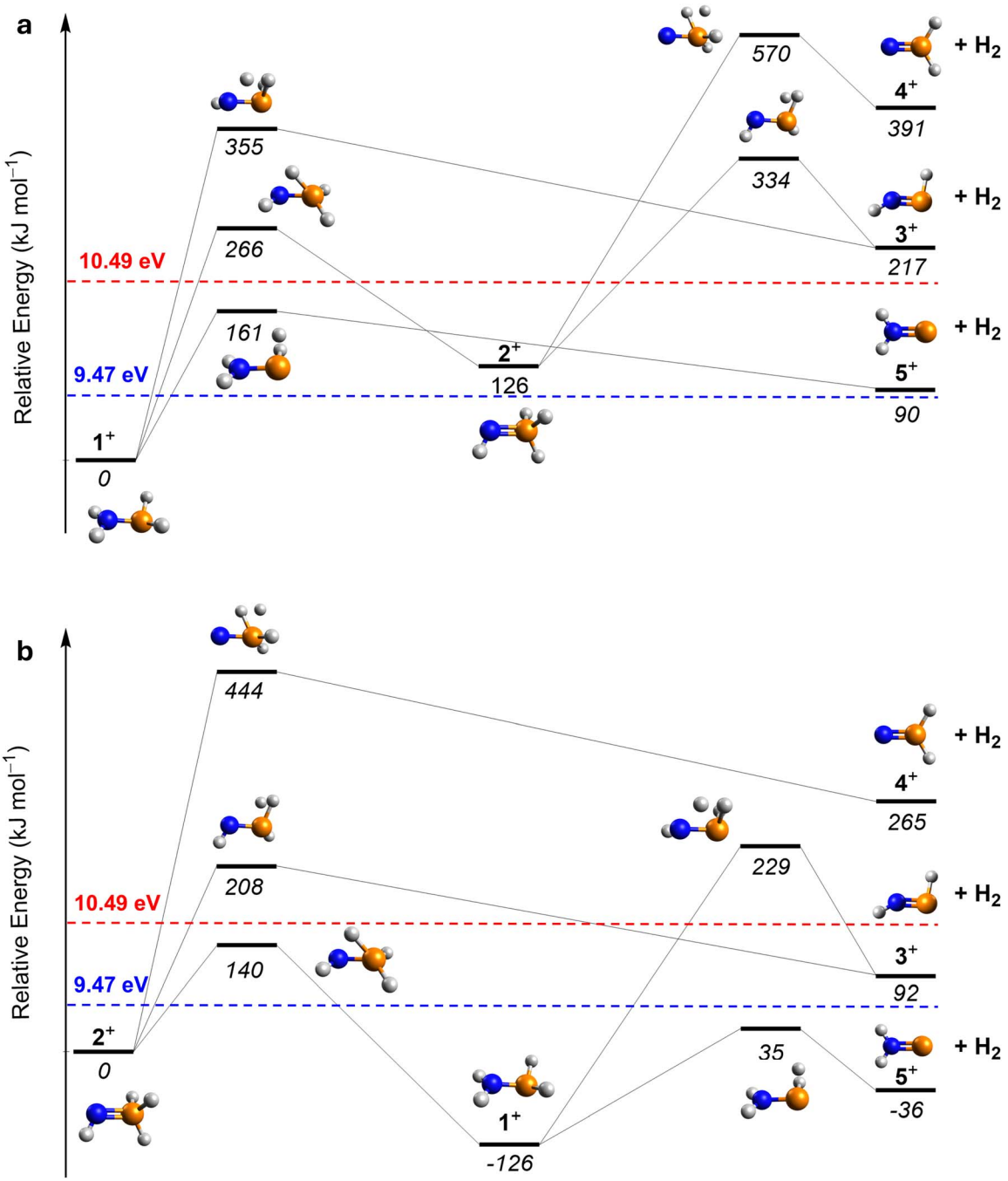

Fig. 4 Calculated dissociation pathways of the phosphinous amide radical cation (**1**$^+$) (a) and phosphine imide radical cation (**2**$^+$) (b). Energies (kJ mol^{-1}) were computed at the CCSD(T)/CBS//CCSD/cc-pVTZ level including zero-point vibrational energy corrections, and are given relative to the corresponding cations. Dashed red and blue lines represent the excess internal energy in the cations **1**$^+$ (a) and **2**$^+$ (b) after photoionization at 10.49 eV and 9.47 eV, respectively.

correspond to molecular formula(e) H_2NP and/or H_5N_3. Replacing the PH_3–NH_3 ice with PH_3–$^{15}NH_3$ ice results in one atomic mass unit (amu) shift of the TPD profile from $m/z = 47$ to 48 indicating the incorporation of only one nitrogen atom. Therefore, the ion signal at $m/z = 47$ from irradiated PH_3–NH_3 ice can be assigned to molecules with the formula H_2NP. Note that the minor sublimation event peaking at around 111 K in the TPD profile of $m/z = 48$ from irradiated PH_3–$^{15}NH_3$ ice is likely caused by the mass shift of N_3H_3 isomers (Fig. S2).[38]

At 10.49 eV, all H_2NP isomers— phosphinimine ((*E*)-**3**, IE = 9.24–9.33 eV; (*Z*)-**3**, IE = 9.43–9.52 eV), phosphinonitrene (**4**; IE = 9.44–9.53 eV), and iminophosphinidene (**5**; IE = 7.45–7.54 eV)—can be ionized (Fig. 1 and Table S2). The ion signal at $m/z = 47$ (H_2NP^+) exhibits sublimation peaks I and II (Fig. 3a), which can be attributed to (*E*)-**3**, (*Z*)-**3**, **4**, and/or **5**. In the gas phase, (*E*)-

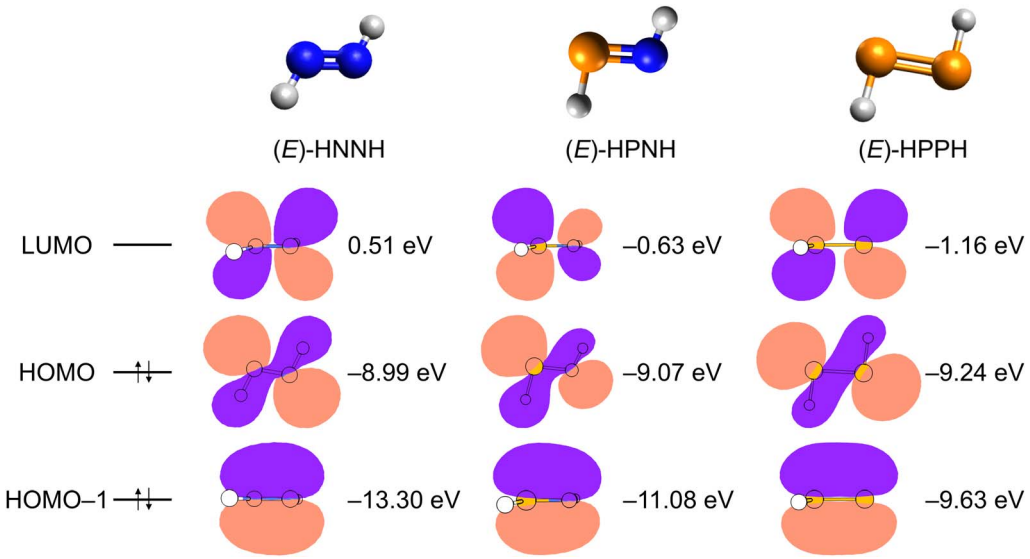

Fig. 5 Calculated frontier molecular orbitals and electronic energies of (*E*)-HNNH, (*E*)-**3**, and (*E*)-HPPH at the ωB97XD/def2TZVPP level of theory. Atoms are color-coded in white for hydrogen, blue for nitrogen, and orange for phosphorus.

3 has the lowest relative energy and is therefore the most stable isomer; isomer **4** is the least stable, lying 154 kJ mol^{-1} above (*E*)-**3**. Upon lowering the photon energy to 9.47 eV, at which (*E*)-**3** (IE = 9.24–9.33 eV) and **5** (IE = 7.43–7.53 eV) can be ionized, whereas (*Z*)-**3** (IE = 9.43–9.52 eV) and **4** (IE = 9.44–9.53 eV) are only accessible near threshold, peak I disappears. Since the IE ranges of (*Z*)-**3** and **4** partially overlap, an additional isomer-selective ultraviolet photolysis experiment was conducted. PH_3–NH_3 ice was first irradiated with energetic electrons to produce H_2NP isomers, followed by ultraviolet (UV) photolysis at 362.8 nm to selectively photodissociate (*Z*)-**3** if formed (Fig. S3). In this electron plus 362.8 nm photolysis experiment recorded at 10.49 eV, the ion signal of $m/z = 47$ (H_2NP^+) reveals that peak I remains (Fig. 3b). The integrated counts of peak I (14394 ± 1081) are comparable to those in the electron only experiment (14106 ± 802), indicating that no evidence of (*Z*)-**3** can be provided. It is worth noting that the TPD profile of peak I of $m/z = 47$ closely resembles that of $m/z = 49$ (Fig. S4), which have been assigned to phosphinous amide (**1**, IE = 8.57 eV) and phosphine imide (**2**, IE = 8.89 eV).[3] Hence, we also explored if peak I could originate from dissociative photoionization of **1** and **2** (49 amu). We computed the dissociation pathways of $\mathbf{1}^+$ and $\mathbf{2}^+$ at the CCSD(T)/CBS//CCSD/cc-pVTZ level of theory. The lowest barriers for the dissociation of $\mathbf{1}^+$ and $\mathbf{2}^+$ are determined to be 161 and 140 kJ mol^{-1}, respectively (Fig. 4). Upon photoionization at 10.49 eV, the excess energies in $\mathbf{1}^+$ (185 kJ mol^{-1}) and $\mathbf{2}^+$ (154 kJ mol^{-1}) exceed these barriers, indicating that peak I originates from isomers **1** and **2** through dissociation of $\mathbf{1}^+$ and $\mathbf{2}^+$. This interpretation is further supported by the absence of peak I at 9.47 eV (Fig. 3c), where the excess energies in $\mathbf{1}^+$ (87 kJ mol^{-1}) and $\mathbf{2}^+$ (56 kJ mol^{-1}) are insufficient to overcome the barriers to dissociation. Therefore, peak I likely originates from the fragment of $\mathbf{1}^+$ and/or $\mathbf{2}^+$ *via* dissociative photoionization. By contrast, peak II is still present when the photon energy was reduced to 9.39 eV, at which only (*E*)-**3** and **5** can be ionized, suggesting that it is attributed to (*E*)-**3** and/or **5**. Further reducing the photon energy to 8.80 eV, where **5** (IE = 7.45–7.54 eV) can be ionized but not (*E*)-**3** (IE = 9.24–9.33 eV), results in the disappearance of peak II, suggesting that peak II is associated with (*E*)-**3**. The detected ion signal of (*E*)-**3** from irradiated PH_3–NH_3 ice was 1910 ± 40 counts at 10.49 eV.

Having provided compelling evidence for the formation of **3** in irradiated phosphine–ammonia ices, we shift focus to their computed electronic and geometric structures. Isomer **3** holds an $^1A'$ electronic ground state and belongs to the C_s point group. In (*E*)-**3**, the HNP and HPN bond angles are 108.9° and 98.6°, respectively (Fig. 1). Compared to (*Z*)-**3**, the bond lengths in (*E*)-**3**—NH (102 pm), NP (159 pm), and PH (143 pm)—differ by less than 2 pm, while the HNP and HPN bond angles are reduced by 6.6° and 6.3°, respectively. The HN=N bond angle and the N=N bond length in *trans*-diazene (HNNH) have been measured to be 106.5° and 125 pm.[39] Compared to *trans*-diazene, phosphorus substitution in (*E*)-**3** reduces the HPN bond angle by 7.9° to 98.6° and lengthens the NP bond length by 34 pm to 159 pm. The longer NP bond length is likely due to the weaker orbital overlap and reduced electronegativity of phosphorus. As nitrogen is replaced by phosphorus, the valence s orbital becomes more strongly contracted relative to the corresponding p orbitals (Fig. 5).[6,40] We calculated the Wiberg bond indices at the ωB97XD/def2TZVPP level of theory in (*E*)-**3**. For phosphorus (P) the Wiberg bond index is 2.77 and for nitrogen (N) 2.70, respectively. For the remaining two hydrogens (Hs) the bond indices are 0.99 (PH) and 0.87 (NH), respectively. The Wiberg bond indices nicely reflect the pnictogen hydrogen single bond and phosphorus nitrogen double bond character. Our natural bond orbital (NBO) calculation reveals pronounced polarization within the P=N double bond, with the nitrogen atom carrying a substantial negative charge (−1.02 e) and the phosphorus atom bearing a corresponding positive charge (+0.76 e). The Kohn–Sham orbitals of (*E*)-HNNH, (*E*)-**3**, and (*E*)-

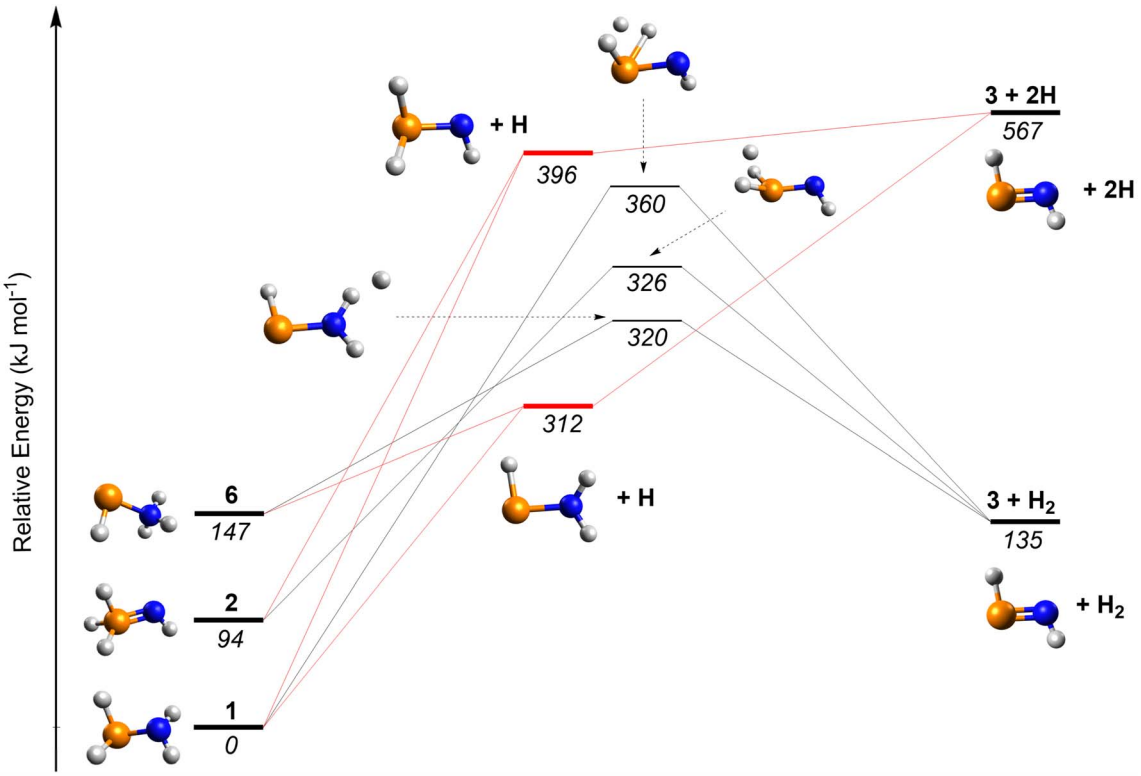

Fig. 6 Potential energy surface leading to **3** through the decomposition of **1**, **2**, and **6** isomers. The energies (italic) were computed at the CCSD(T)/CBS//CCSD/cc-pVTZ level including CCSD/cc-pVTZ zero-point vibrational energy corrections.

HPPH are depicted together with their electronic energies in eV in Fig. 5. The LUMO orbitals in (*E*)-HNNH, (*E*)-**3**, and (*E*)-HPPH correspond to the antibonding π* orbital between the two corresponding pnictogens. The HOMO orbitals mainly depict the lone-pair character on the phosphorus and nitrogen atom(s), respectively. The pnictogen–pnictogen double bond is reflected by the HOMO–1 π bonding orbital. The energy differences between the highest-occupied molecular orbital (HOMO) and lowest-unoccupied molecular orbital (LUMO) are 9.50 eV in (*E*)-HNNH, 8.44 eV in (*E*)-**3**, and 8.08 eV in (*E*)-HPPH, respectively. The LUMO energy of (*E*)-HNNH is positive, while it is negative in (*E*)-**3**, and even more negative in (*E*)-HPPH.

We now consider potential formation pathways to **3**. Barrierless radical–radical recombination between the phosphino radical (PH_2) and the amino radical (NH_2) leads to the formation of phosphinous amide (**1**), which can isomerize to phosphine imide (**2**) and iminophosphine ($HPNH_3$, **6**) *via* reaction barriers of 308 and 244 kJ mol^{-1}, respectively, calculated at the CCSD(T)/CBS//B3LYP/cc-pVTZ level of theory.[3] Note that evidence for the formation of hydrazine (N_2H_4) and diphosphine (P_2H_4) have been provided (Fig. S5, SI). Previous studies have revealed their formation in electron-irradiated ammonia- and phosphine-containing ices *via* the recombination of two NH_2 and two PH_2 radicals, respectively.[41,42] Upon interaction with energetic electrons, **3** can be formed from the corresponding H_4NP isomers *via* two atomic hydrogen (H) losses or a single molecular hydrogen (H_2) loss (Fig. 6). The potential energy surface was calculated at the CCSD(T)/CBS//CCSD/cc-pVTZ level including zero-point vibrational energy corrections. The unimolecular decomposition of **1**, **2**, and **6** yields (*E*)-**3** by loss of two hydrogen atoms, which are endoergic by 567, 473, and 420 kJ mol^{-1}, respectively. Alternatively, the molecular hydrogen elimination of **1**, **2**, and **6** can lead to (*E*)-**3** through three transition states, which are located 360, 232, and 173 kJ mol^{-1} above the corresponding reactants, respectively. Notably, the H_2-elimination pathway from **6** exhibits the lowest barrier with an exoergicity of 12 kJ mol^{-1}. The interconversion barrier from (*Z*)-**3** to (*E*)-**3** is calculated to be 70 kJ mol^{-1} at the QCISD/LANL2DZdp level of theory.[6] These energies can be supplied by energetic electrons during space-simulation or secondary electrons produced by GCRs in interstellar environments.

Conclusion and outlook

Altogether, the present work reports the first formation of (*E*)-phosphinimine ((*E*)-**3**)—the simplest iminophosphane—in low-temperature phosphine–ammonia astrophysical model ices. The ice mixtures were exposed to energetic electrons, simulating the effects of secondary electrons produced by GCRs in cold molecular clouds. Isomer (*E*)-**3** was identified in the gas phase for the first time during TPD utilizing PI-ReToF-MS with their formulas verified with isotopic labeling. Assuming a Maxwell–Boltzmann velocity distribution for thermally desorbing species from the ices,[43] isomer (*E*)-**3** subliming at 153 K is estimated to have an average molecular velocity of 261 m s^{-1}; considering the 2.0 ±

0.5 mm distance between the ice surface and the photoionization region, the gas-phase lifetime for neutral (*E*)-**3** exceeds 7.6 ± 1.9 μs. In astrophysical environments, low temperatures of around 10 K, lower densities, and reduced collision frequencies are expected to significantly extend its lifetime. These results reveal key formation pathways for (*E*)-**3**, highlighting the critical role of GCR-driven non-equilibrium chemistry in the formation of phosphorus–nitrogen molecules in interstellar environments. Phosphine has been detected in the ISM towards carbon-rich asymptotic giant branch (AGB) envelope and protoplanetary nebula with abundances reaching up to 4×10^{-7} relative to molecular hydrogen.[29,30] On interstellar grains, phosphine is believed to form efficiently through successive hydrogenation of atomic phosphorus.[17,31] Ammonia is widely present in interstellar ices with estimated abundances of up to 15% relative to water.[33] Our results suggest that the hitherto astronomically unobserved (*E*)-**3** can form in interstellar ices containing phosphine and ammonia, representing a potential target for future astronomical detection. We note that the phosphine–ammonia ice mixture serves as a model system to investigate low-temperature reaction pathways leading to (*E*)-**3**, rather than to reproduce the exact relative composition of interstellar ices. Given that water is the dominant component of interstellar ices,[44] future studies should explore its formation pathways in more complex ice mixtures incorporating water. In irradiated phosphine–ammonia–water ices, hydroxyl (OH) radical formed from water may react with phosphino and amino radicals to form phosphinous acid (PH_2OH)[20] and hydroxylamine (NH_2OH),[41] respectively, thereby competing with reaction pathways leading to **1**, **2**, and **6**, which serve as precursors to (*E*)-**3**. Once synthesized in cold molecular clouds, it can be trapped and stabilized within low-temperature ices due to the limited mobility, potentially leading to the formation of biologically relevant phosphorus-containing species upon processing by ionizing sources such as UV photons and GCRs; for instance, it may serve as a key precursor to prebiotic phosphorylating reagents such as amidophosphonate and diamidophosphate.[21] A fraction of these compounds could become embedded into planetesimals during the star forming and may eventually be delivered to planets such as early Earth *via* cometary or meteoritic impacts,[45] thereby facilitating phosphorylation reactions on the prebiotic Earth.[46,47] Finally, both phosphine and ammonia have been detected in the atmospheres of gas giant planets such as Saturn and Jupiter,[48,49] our results may provide valuable insights into the phosphorus–nitrogen chemistry in planetary environments as well.

Author contributions

R. I. K. designed the experiments; J. W., A. B., Z. W., M. M., and J. H. M. performed the experiments; J. W. analyzed the data; B.-J. S., A. H. H. C., and A. K. E. conducted the theoretical analysis; the manuscript was written by J. W., A. K. E., and R. I. K.

Conflicts of interest

The authors declare no competing financial interest.

Data availability

Essential data are provided in the article and the supporting information (SI). Additional data are available from the corresponding author upon reasonable request. Supplementary information: methods (Experimental and Computational), FTIR spectra and assignments, TPD profiles of PH_3–NH_3 ice measured at 10.49 eV, simulated ultraviolet-visible spectra, IEs and relative energies, VUV light generation parameters, and optimized Cartesian coordinates, harmonic frequencies, infrared intensities, and T_1 diagnostic values for calculated structures. See DOI: https://doi.org/10.1039/d6sc01818a.

Acknowledgements

We thank the support by the U.S. National Science Foundation (NSF), Division of Astronomical Sciences, through grant AST-2403867 (R. I. K.). B.-J. S. and A. H. H. C. gratefully acknowledge the National Center for High-performance Computer in Taiwan for providing computational resources. The calculations in Bochum (A. K. E) were funded by the Deutsche Forschungsgemeinschaft (DFG, German Research Foundation) under Germany's Excellence Strategy – EXC 2033 – 390677874 – RESOLV.

References

1 B. E. Turner and J. Bally, *Astrophys. J.*, 1987, **321**, L75.
2 L. M. Ziurys, *Astrophys. J.*, 1987, **321**, L81.
3 C. Zhu, A. Bergantini, S. K. Singh, R. I. Kaiser, A. K. Eckhardt, P. R. Schreiner, Y.-S. Huang, B.-J. Sun and A. H. H. Chang, *Chem. Commun.*, 2021, **57**, 4958–4961.
4 C. Zhu, A. M. Turner, M. J. Abplanalp, R. I. Kaiser, B. Webb, G. Siuzdak and R. C. Fortenberry, *Astrophys. J.*, 2020, **899**, L3.
5 M. Fernández-Ruz, I. Jiménez-Serra and J. Aguirre, *Astrophys. J.*, 2023, **956**, 47.
6 C.-H. Lai, M.-D. Su and S.-Y. Chu, *J. Phys. Chem. A*, 2003, **107**, 2700–2710.
7 H. S. P. Müller and D. E. Woon, *J. Phys. Chem. A*, 2013, **117**, 13868–13877.
8 L. Baptista and A. A. de Almeida, *J. Phys. Chem. A*, 2023, **127**, 1000–1012.
9 J. Jiang, L. Huang, B. Zhu, W. Fan, L. Wang, I. Y. Zhang, W. Fang, T. Trabelsi, J. S. Francisco and X. Zeng, *Angew. Chem., Int. Ed.*, 2025, **64**, e202414456.
10 E. Niecke and D. Gudat, *Angew. Chem., Int. Ed. Engl.*, 1991, **30**, 217–237.
11 J. Jiang, Y. Guo, L. Huang, L. Wang, G. Rauhut and X. Zeng, *Nat. Commun.*, 2026, **17**, 1687.
12 K. Altwegg, H. Balsiger, A. Bar-Nun, J.-J. Berthelier, A. Bieler, P. Bochsler, C. Briois, U. Calmonte, M. R. Combi, H. Cottin, J. De Keyser, F. Dhooghe, B. Fiethe, S. A. Fuselier, S. Gasc, T. I. Gombosi, K. C. Hansen, M. Haessig, A. Jäckel, E. Kopp, A. Korth, L. Le Roy, U. Mall, B. Marty, O. Mousis, T. Owen, H. Rème, M. Rubin, T. Sémon, C.-Y. Tzou, J. Hunter Waite and P. Wurz, *Sci. Adv.*, 2016, **2**, e1600285.
13 F. Fontani, *Front. Astron. Space Sci.*, 2024, **11**, 1451127.

14 B. A. McGuire, *Astrophys. J., Suppl. Ser.*, 2022, **259**, 30.
15 L. M. Ziurys, *Annu. Rev. Phys. Chem.*, 2024, **75**, 307–327.
16 J. García de la Concepción, C. Cavallotti, V. Barone, C. Puzzarini and I. Jiménez-Serra, *Astrophys. J.*, 2024, **963**, 142.
17 V. M. Rivilla, M. N. Drozdovskaya, K. Altwegg, P. Caselli, M. T. Beltrán, F. Fontani, F. F. S. van der Tak, R. Cesaroni, A. Vasyunin, M. Rubin, F. Lique, S. Marinakis, L. Testi and t. R. team, *Mon. Not. R. Astron. Soc.*, 2020, **492**, 1180–1198.
18 G. W. Cooper, W. M. Onwo and J. R. Cronin, *Geochim. Cosmochim. Acta*, 1992, **56**, 4109–4115.
19 P. R. Heck, J. Greer, L. Kööp, R. Trappitsch, F. Gyngard, H. Busemann, C. Maden, J. N. Ávila, A. M. Davis and R. Wieler, *Proc. Natl. Acad. Sci. U. S. A*, 2020, **117**, 1884–1889.
20 A. M. Turner, A. Bergantini, M. J. Abplanalp, C. Zhu, S. Góbi, B.-J. Sun, K.-H. Chao, A. H. H. Chang, C. Meinert and R. I. Kaiser, *Nat. Commun.*, 2018, **9**, 3851.
21 M. Karki, C. Gibard, S. Bhowmik and R. Krishnamurthy, *Life*, 2017, **7**, 32.
22 G. Hajos and I. Nagy, *Curr. Org. Chem.*, 2008, **12**, 39–58.
23 K. Pedrood, M. N. Montazer, B. Larijani and M. Mahdavi, *Synthesis*, 2021, **53**, 2342–2366.
24 C. Zhu, A. K. Eckhardt, S. Chandra, A. M. Turner, P. R. Schreiner and R. I. Kaiser, *Nat. Commun.*, 2021, **12**, 5467.
25 C. Zhu, A. K. Eckhardt, A. Bergantini, S. K. Singh, P. R. Schreiner and R. I. Kaiser, *Sci. Adv.*, 2020, **6**, eaba6934.
26 B. Lu and X. Zeng, *Chem. Eur J.*, 2024, **30**, e202303283.
27 B. C. Ferrari, K. Slavicinska and C. J. Bennett, *Acc. Chem. Res.*, 2021, **54**, 1067–1079.
28 A. G. Yeghikyan, *Astrophysics*, 2011, **54**, 87–99.
29 E. D. Tenenbaum and L. M. Ziurys, *Astrophys. J.*, 2008, **680**, L121–L124.
30 M. Agúndez, J. Cernicharo, L. Decin, P. Encrenaz and D. Teyssier, *Astrophys. J. Lett.*, 2014, **790**, L27.
31 I. Jiménez-Serra, S. Viti, D. Quénard and J. Holdship, *Astrophys. J.*, 2018, **862**, 128.
32 M. K. McClure, W. R. M. Rocha, K. M. Pontoppidan, N. Crouzet, L. E. U. Chu, E. Dartois, T. Lamberts, J. A. Noble, Y. J. Pendleton, G. Perotti, D. Qasim, M. G. Rachid, Z. L. Smith, F. Sun, T. L. Beck, A. C. A. Boogert, W. A. Brown, P. Caselli, S. B. Charnley, H. M. Cuppen, H. Dickinson, M. N. Drozdovskaya, E. Egami, J. Erkal, H. Fraser, R. T. Garrod, D. Harsono, S. Ioppolo, I. Jiménez-Serra, M. Jin, J. K. Jørgensen, L. E. Kristensen, D. C. Lis, M. R. S. McCoustra, B. A. McGuire, G. J. Melnick, K. I. Öberg, M. E. Palumbo, T. Shimonishi, J. A. Sturm, E. F. van Dishoeck and H. Linnartz, *Nat. Astron.*, 2023, **7**, 431–443.
33 E. L. Gibb, D. C. B. Whittet, A. C. A. Boogert and A. G. G. M. Tielens, *Astrophys. J., Suppl. Ser.*, 2004, **151**, 35–73.
34 J. H. Teles, G. Maier, B. Andes Hess Jr and L. J. Schaad, *Chem. Ber.*, 1989, **122**, 749–752.
35 G. Socrates, *Infrared and raman characteristic group frequencies: Tables and charts*, John Wiley & Sons, Ltd, New York, 3rd edn, 2004.
36 J. Wang, C. Zhang, J. H. Marks, M. M. Evseev, O. V. Kuznetsov, I. O. Antonov and R. I. Kaiser, *Nat. Commun.*, 2024, **15**, 10189.
37 A. M. Turner and R. I. Kaiser, *Acc. Chem. Res.*, 2020, **53**, 2791–2805.
38 M. Förstel, Y. A. Tsegaw, P. Maksyutenko, A. M. Mebel, W. Sander and R. I. Kaiser, *ChemPhysChem*, 2016, **17**, 2726–2735.
39 M. Carlotti, J. W. C. Johns and A. Trombetti, *Can. J. Phys.*, 1974, **52**, 340–344.
40 W. Kutzelnigg, *Angew. Chem., Int. Ed. Engl.*, 1984, **23**, 272–295.
41 W. Zheng and R. I. Kaiser, *J. Phys. Chem. A*, 2010, **114**, 5251–5255.
42 A. M. Turner, M. J. Abplanalp, S. Y. Chen, Y. T. Chen, A. H. H. Chang and R. I. Kaiser, *Phys. Chem. Chem. Phys.*, 2015, **17**, 27281–27291.
43 J. Wang, J. H. Marks, A. M. Turner, A. M. Mebel, A. K. Eckhardt and R. I. Kaiser, *Sci. Adv.*, 2023, **9**, eadg1134.
44 A. C. A. Boogert, P. A. Gerakines and D. C. B. Whittet, *Annu. Rev. Astron. Astrophys.*, 2015, **53**, 541–581.
45 G. Cooper, N. Kimmich, W. Belisle, J. Sarinana, K. Brabham and L. Garrel, *Nature*, 2001, **414**, 879–883.
46 R. Krishnamurthy, S. Guntha and A. Eschenmoser, *Angew. Chem., Int. Ed.*, 2000, **39**, 2281–2285.
47 M. Gull, H. A. Cruz, R. Krishnamurthy and M. A. Pasek, *Commun. Chem.*, 2025, **8**, 187.
48 L. N. Fletcher, G. S. Orton, N. A. Teanby and P. G. J. Irwin, *Icarus*, 2009, **202**, 543–564.
49 J. H. Woodman, L. Trafton and T. Owen, *Icarus*, 1977, **32**, 314–320.